EXTREME MECHANICS
LETTERS

Description of the image

Mechanics of a pressure-controlled adhesive membrane for soft robotic gripping on curved surfaces

Check for updates

Sukho Song [a,b], Dirk-M. Drotlef [b], Jamie Paik [a], Carmel Majidi [c], Metin Sitti [b,d,*]

[a] Reconfigurable Robotics Laboratory, École Polytechnique Fédérale de Lausanne, Station 9, 1015 Lausanne, Switzerland
[b] Physical Intelligence Department, Max Planck Institute for Intelligent Systems, 70569 Stuttgart, Germany
[c] Department of Mechanical Engineering and Robotics Institute, Carnegie Mellon University, Pittsburgh, PA 15213, United States
[d] School of Medicine and School of Engineering, Koç University, 34450 Istanbul, Turkey

GRAPHICAL ABSTRACT
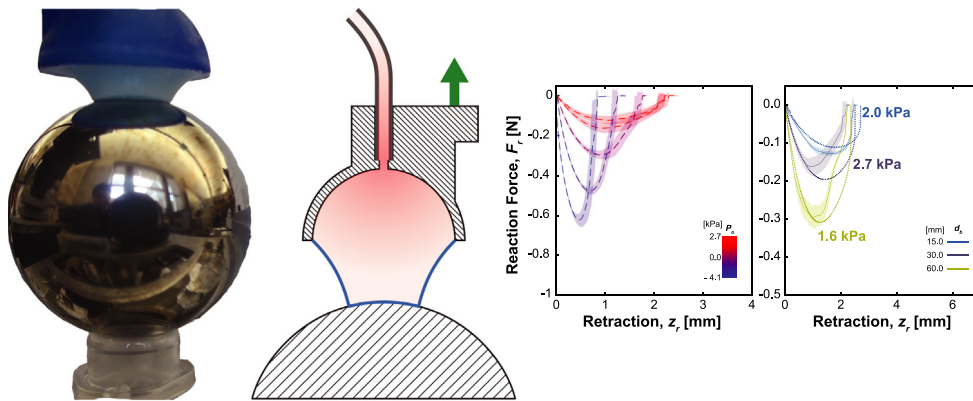
HIGHLIGHTS

- Fracture mechanics on pull-off of a pressurized membrane on 3D surfaces is studied.
- A negative pressure differential causes the effect same as the membrane is stiffened.
- Size and curvature of contact interfaces influence on adhesion profiles.
- Model predictions show good agreements with pull-off forces in experiments.

ARTICLE INFO

ABSTRACT

This paper aims at understanding the adhesion mechanics of a pressure-controlled adhesive thin elastomeric membrane for soft robotic gripping on non-planar, curved surfaces. The adhesive elastic membrane is lined with gecko-inspired microfiber arrays and can be inflated or deflated by controlled internal air pressure. Previous studies with the soft robotic grippers using dry adhesives showed repeatable adhesion and transfer printing of various non-planar objects with high reliability. In this study, we perform experimental characterization and theoretical analysis to better understand the influence of size and shape of the adhering curved objects on the range of internal air pressures as well as the force profile. In addition, decrease in the internal air pressure results in an increased pull-off force associated with a change in the range of gripper retraction for pulling off the membrane on various curved surfaces. An approximate analytical model dealing with the complex boundary conditions presented in this paper can provide quantitative estimates of pull-off forces for a wide

* Corresponding author at: Physical Intelligence Department, Max Planck Institute for Intelligent Systems, 70569 Stuttgart, Germany.
E-mail address: sitti@is.mpg.de (M. Sitti).

Transfer printing

variety of surface curvatures and internal air pressures, as well as qualitative understanding of how force profiles change under moderate pressure differentials.

1. Introduction

Understanding the fracture mechanics of an elastic membrane plays a critical role in adhesion and thin film sciences [1] involved in many scientific and engineering problems, such as surface attachment and detachment during animal locomotion [2–5], cell-to-cell adhesion [6–8], transfer printing [9–12], and adhesion-based soft robotic devices [13–18]. Previous efforts have investigated various contact problems for an elastic membrane with relatively simple boundary conditions. For example, Flory [19], Long [20,21], Xu [22], Laprade [23], and Srivastava [24] et al. performed studies where they fixed a membrane at a specific distance from a flat substrate and used pneumatic inflation to attach and detach the membrane from the substrate. Shanahan [25], Wan [26], Majidi [27], Shi [28], and Ju [29] et al. placed a membrane under ambient air pressure, while bringing the membrane into contact or peeling it off from the substrate. Patil [30,31] and Springman [32] et al. focused on adhesion mechanics of a membrane on irregular or deformable surfaces, but did not take the simultaneous movement of the contact interface and change in air pressure into account. To the best of our knowledge, there is no previous work that fully accounts for all of these boundary conditions (i.e., moving the contact interface, internal pressure change, and non-planar surfaces), while such complex boundary conditions occur commonly in most membrane adhesion applications in the real world. For example, pulling membranous biological tissues apart often involves hydrostatic pressure change due to deformation of the biological membrane and this influences the interfacial fracture strength. In a recent study, we showed that an adhesion-based soft robotic gripper can use changes in internal pressure to control interfacial stress of a membrane and perform pick and place manipulation of various objects with different sizes and shapes [33].

In this paper, we aim at understanding the mechanics of membrane adhesion undergoing more complex boundary conditions using experimental methods and an analytical model presented in our previous works [33–35]. In particular, we focus on peeling of a membrane covered with fibrillar adhesives from a spherical surface when subject to a combined pull-off force and negative pressure differential. Gecko-inspired fibrillar adhesives with mushroom-shaped tips are integrated with a soft elastomeric membrane using a technique demonstrated by Murphy et al. [36–38]. Normal force profiles of the adhering membrane are investigated to study the effect of substrate geometry and internal pressure change on the membrane adhesion. In order to predict the behavior of the membrane and the pull-off forces under complex boundary conditions, we developed an approximate analytical model based on the principle of minimum potential energy capable of dealing with the given complex boundary conditions, and discussed its ability and current limitations.

2. Methods

For attaching to diverse curved surfaces, we use a fibrillar adhesives on a membrane (FAM) architecture in which an elastic membrane is covered with gecko-inspired synthetic microfiber adhesives as shown in Fig. 1b. This design offers key advantages for robust and reversible adhesion since: (i) fibrillar structures maximize the effective work of adhesion of the membrane, significantly enhancing the attachment performance; (ii) fibrillar

surface can be cleaned easily and reused over repetitive pick-and-place cycles as demonstrated in [39–41]; (iii) gaps between microfibers on the membrane allow the air to flow through the contact interface, preventing suction or other unwanted forces from affecting the adhesion testing.

Two FAMs are prepared with different materials; one is fully made of poly-dimethylsiloxane (PDMS) [35], while the other uses two polyurethanes, ST-1060 (BJB Enterprises, Inc.) for the microfibers and F-25 (BJB Enterprises, Inc.) for the membrane [33, 34]. The ST-1060 polyurethane microfiber adhesives were also fabricated on a rigid acrylic punch (Fiber Adhesives on Rigid Punch, FARP) for visualizing the effect of backing stiffness in Fig. 3e and f, together with the polyurethane-based FAM. Both of the polyurethane-based FAM and FARP implementations have an approximately 75 μm thick backing membrane with 105 μm in diameter microfiber adhesives, while the PDMS-based FAM consists of a 200 μm thick backing layer with 50 μm diameter microfibers. All the FAM and FARP implementations have 16 mm diameter. The FAM is attached on a 3D-printed gripper body (Fig. 1a) and fixed to a force transducer (GSO-25, GSO-500, and GSO-1K Transducer Techniques LLC, 7 in Fig. 1c). The approach and retraction of the membrane from the substrate (6 in Fig. 1c) is controlled by a motorized z-axis stage (LPS-65 2" Physik Instrumente GmbH & Co. KG, 8 in Fig. 1c). Internal pressure of the FAM is regulated by a syringe pump (Legato 210P, KDScientific Inc., 1 in Fig. 1c). The corresponding internal pressure is measured by a pressure sensor (HSCSANN600MDAA5, Honeywell International Inc., 3 in Fig. 1c) with respect to retraction of the gripper and recorded by a customized data processing code.

Fig. 2 shows an experimental sequence (Fig. 2c) as well as corresponding reaction force (F_r) and internal pressure (P_a) profiles (Fig. 2a and b) of the FAM and the gripper body. First, the gripper is brought in contact with a spherical glass surface (step 1), until the membrane undergoes a specific preload force between 0.5–1.0 N, which varies depending on surface curvature and size of the sphere (step 2). After changing the internal pressure by the syringe pump (step 3), the gripper is slowly retracted with 10 μm/s retraction speed (step 4) until the membrane completely peels off from the substrate (step 6). Here, the internal pressure in step 4 is defined as the initial pressure (P_0). Compression force is shown as a positive reaction force in Fig. 2a, while a negative reaction force indicates tensile force by adhesion. The reaction force starts decreasing during gripper retraction from the substrate and crosses the force equilibrium $F_r = 0$. Here, the position of the gripper relative to the force equilibrium is defined as the retraction (z_r), and a travel distance until full detachment is defined as pull-off distance (D_p) (or retraction at $F_r = 0$ in Fig. 2b). Note that the air pressure in Fig. 2b decreases during retraction, as volume inside the gripper body expands due to the deformation of the FAM. The reaction force reaches its minimum at step 5, providing the maximum adhesion, which is defined as the pull-off force (F_p) in Fig. 2b. After step 5, the reaction force increases as the contact area decreases during retraction, until the membrane is fully detached from the substrate at step 6.

3. Experimental results

Fig. 3a, b, c and d show reaction force (F_r) profiles of the PDMS-based FAM with respect to the retraction (z_r), depending on diameter of spherical glass surfaces (d_b) and initial pressure
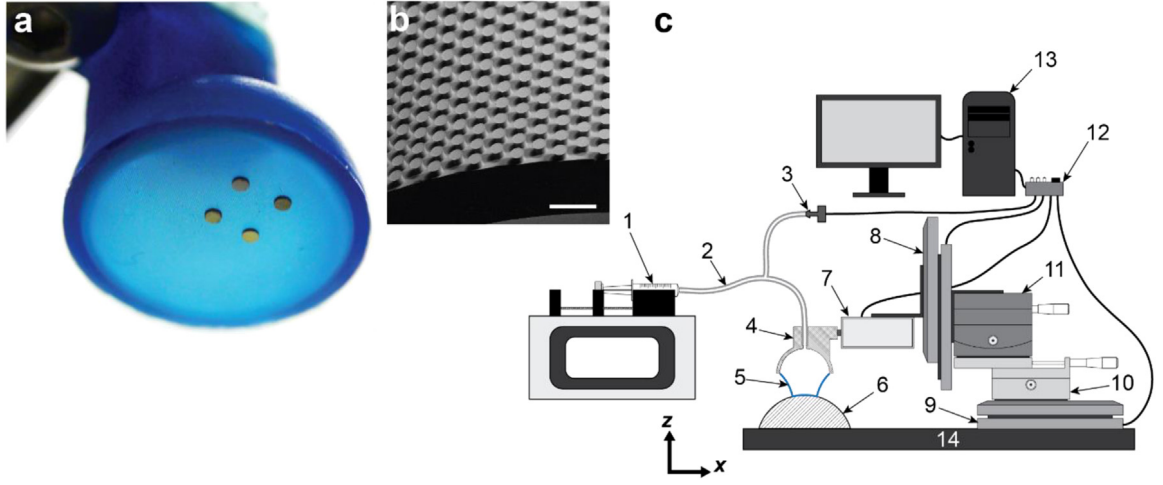
Fig. 1. An adhesion-based robotic soft gripper with gecko-inspired fiber adhesives on a membrane (FAM) design and schematics of the adhesion test setup: **(a)** The polyurethane-based FAM demonstrating adhesion of four silicon disks (1 mm in diameter). **(b)** SEM image of cross-sectional view of the PDMS-based FAM patterned with microfiber adhesives. The scale bar indicates 200 μm. **(c)** A schematic of a customized adhesion test setup characterizing force profiles of the FAM with various boundary conditions (1: syringe pump, 2: tubing, 3: pressure sensor, 4: pressure chamber, 5: FAM, 6: glass sphere, 7: force transducer, 8: motorized stage (z-axis), 9: motorized stage (x-axis), 10: manual stage, 11: goniometer, 12: DAQ, 13: computer).
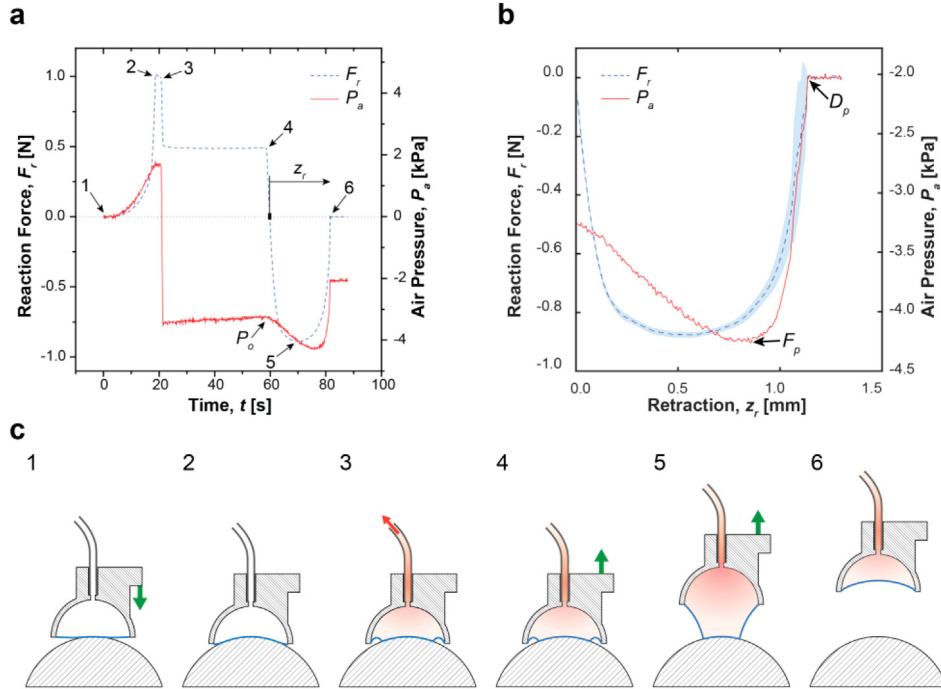

Fig. 2. Experimental attachment and detachment characterization of the FAM on a spherical glass surface: **(a)** Reaction force (F_r in blue dashed-line) and air pressure (P_a in red straight-line) profiles of a PDMS-based FAM with respect to time lapse (t). Diameter of the spherical glass surface is 60 mm, and applied initial pressure (P_0) is approximately −3.2 kPa. Numbers correspond to experimental sequences in (c). **(b)** Reaction force (F_r) and air pressure (P_a) profiles of experiments in (a) with respect to retraction (z_r). Shaded areas represent standard deviations of 5 experiments. **(c)** Schematics of the experimental sequence. Numbers match with force profiles shown in (a), 1: contact, 2: preload, 3: applying negative pressure differential, 4: retraction, 5: pull-off, 6: detachment.

(P_0). The membrane shows different ranges of internal pressure depending on glass sphere diameters ranging from $d_b = 15$ mm to $d_b = 60$ mm. $d_b = 30$ mm undergoes the widest range of P_0 ranging from $P_0 = 2.7$ kPa to $P_0 = -4.1$ kPa as seen in Fig. 3b. As the membrane curves into the gripper when exposed to a high negative pressure differential as illustrated in **Fig. S1a**, we speculated that the shape mismatch between the inward curvature of the FAM and the curved surface could be minimized at $d_b = 30$ mm as shown in **Fig. S1b** with the smallest stress concentration on the contact interface among the examined sphere diameters.

Fig. 3a and c also show that the overall pull-off force (F_p) increases with respect to the size of the glass spheres, as well as with decreased initial pressure (P_0). In case of $d_b = 60$ mm, a reduction in P_0 leads to an increase in magnitude of the pull-off force (F_p) from 0.30 N to 0.88 N, as well as a decrease in the pull-off distance (D_p) from 2.24 mm to 1.14 mm, respectively. For $d_b = 15$ mm, the magnitude of F_p increases from 0.13 N to 0.15 N with respect to the reduction in P_0 from 2.0 kPa to −0.7 kPa, while D_p first slightly increases from 2.48 mm to 2.55 mm, then decreases to 2.21 mm. Overall, the general trend of a greater magnitude of F_p together with shorter D_p is observed with respect
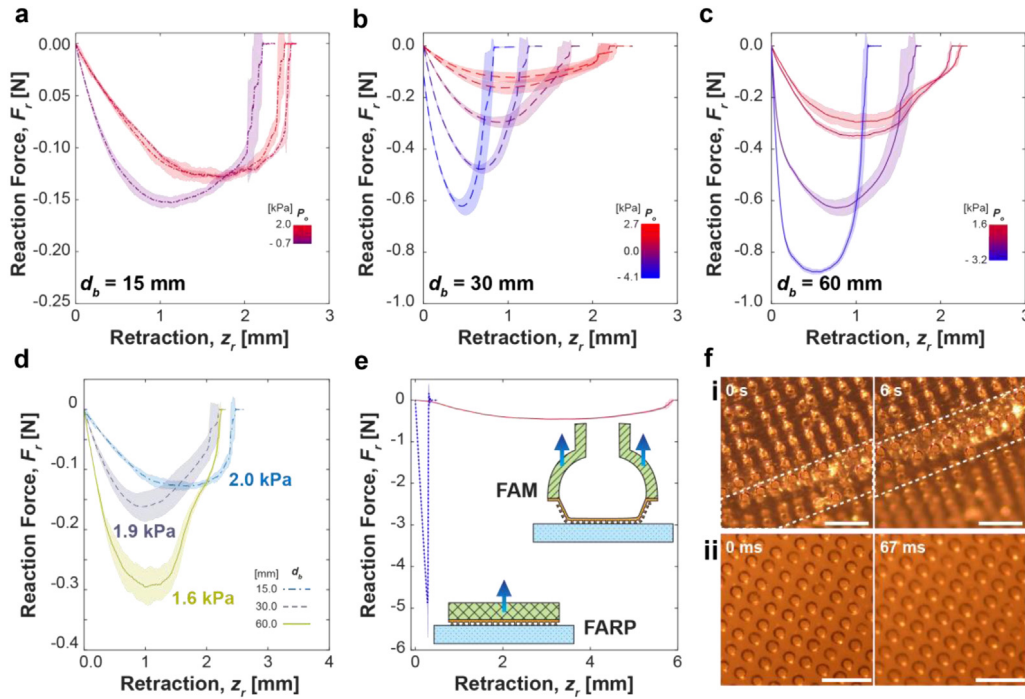
Fig. 3. Reaction force (F_r) profiles of the PDMS-based FAM with respect to retraction (z_r), depending on different initial pressures (P_0) and on spherical glass surfaces with diameter of (**a**) $d_b = 15$ mm, (**b**) $d_b = 30$ mm, and (**c**) $d_b = 60$ mm. (**d**) Reaction force profiles of the PDMS-based FAM with respect to retraction, depending on diameter of spheres under similar positive pressure conditions. Pressure values in the figure indicate the corresponding initial pressures. (**e**) Reaction force profiles of the polyurethane-based FAM and FARP with respect to retraction on flat glass substrate. (**f**) Microscopic contact images of the polyurethane-based FAM (**i**) and FARP (**ii**) during the gripper retraction from a flat glass substrate. While the FAM shows a clear peel-zone (indicated by two dashed lines) slowly receding from the contact edge, all microfibers of the FARP detached within 67 ms. All shaded areas represent standard deviations of 3–5 measurements, and the scale bar indicates 1 mm.

to the increase in negative P_0, which is similar to the force profiles when a rigid backing supports the fibrillar adhesives as seen in Fig. 3e. All microfibers are simultaneously pulled off from a planar substrate (Fig. 3f-ii), exerting high adhesion, since equal load sharing condition is achieved by the rigid backing. The area encircled by the force profiles in Fig. 3e corresponds to the total adhesion energy during pull-off. Comparing these values suggests that the rigid backing helps to concentrate the total adhesion energy within a short range of retraction, resulting in higher fracture strength. When the microfibers are backed with a soft membrane (Fig. 3f-i), on the other hand, a long range retraction dissipates the same total adhesion energy associated with approximately 10 times smaller pull-off force. Without actually stiffening the backing layer, however, the decrease in the internal gripper pressure causes a *pseudo*-effect as if the membrane backing layer is stiffened. The adhesion energy is concentrated within a shorter retraction range by more uniform load distribution, and exerting a higher pull-off force on a wide range of curved substrates.

Fig. 3d shows the effect of the substrate geometry on the shape of reaction force profiles. Under similar pressure conditions, the PDMS-based FAM on $d_b = 60$ mm approaches F_p at 45% of D_p ($z_r = 1.0$ mm for F_p), while the FAM on $d_b = 15$ mm has to be retracted up to 70% of D_p ($z_r = 1.7$ mm for F_p). When adhering to a small sphere, most of the FAM is not in contact with the substrate as shown in Fig. 4a. Long retraction for stretching the FAM is required to induce high pulling stress at the circumferential contact line and initiate peeling of the membrane. In this case, area of the membrane being actively pulled off a surface, known as peel-zone [3], accounts for a high fraction of the entire contact area. Once the circumferential contact edge reaches its critical fracture strength, the entire contact is pulled off simultaneously. When engaging a large sphere, on the other hand, almost the entire FAM is in contact with the sphere surface

as shown in Fig. 4b. Conversely, the peel-zone does not account for a high fraction of the entire contact area, consequently initiating gradual peel-off the membrane within a short retraction of the gripper. Moreover, the peeling angle between the FAM and tangential direction of the spherical surface also affects the shape of the force profile as reported by Kendall [1], exerting a higher pull-off force with a smaller peeling angle. The transition from instantaneous 'pull-off' to gradual 'peel-off' of a membrane with the increased d_b is in agreement with our experimental results with the polyurethane-based FAM as shown in **Fig. S2**.

4. Theoretical model

An approximate theoretical model to predict the pull-off force and reaction force profile based on the principle of the minimum potential energy was first proposed in [33] and was further developed in [35] to consider the effect of non-planar geometries and pressure change. One limitation of the previous model is that deformation of the adhering membrane in contact is considered to be negligible. In this work, we propose an improved model taking the effect of deformation of the contacting membrane into account and discuss how the new model performs in predicting the pull-off force compared to the earlier model.

The model is developed to deal simultaneously with the three boundary conditions — retraction, internal pressure, and non-planar spherical surfaces. Other membrane theories [20–22,42] typically estimate the deformation of the membrane with a series of derivations based on balance laws and the constitutive equations for a hyperelastic film. In contrast, our model approximates the shape of the deformed membrane as a truncated cone. Although it makes the model simpler and easy to calculate, this assumption undoubtedly influences the model's accuracy, which will be discussed in Fig. 5. As described in [35], several
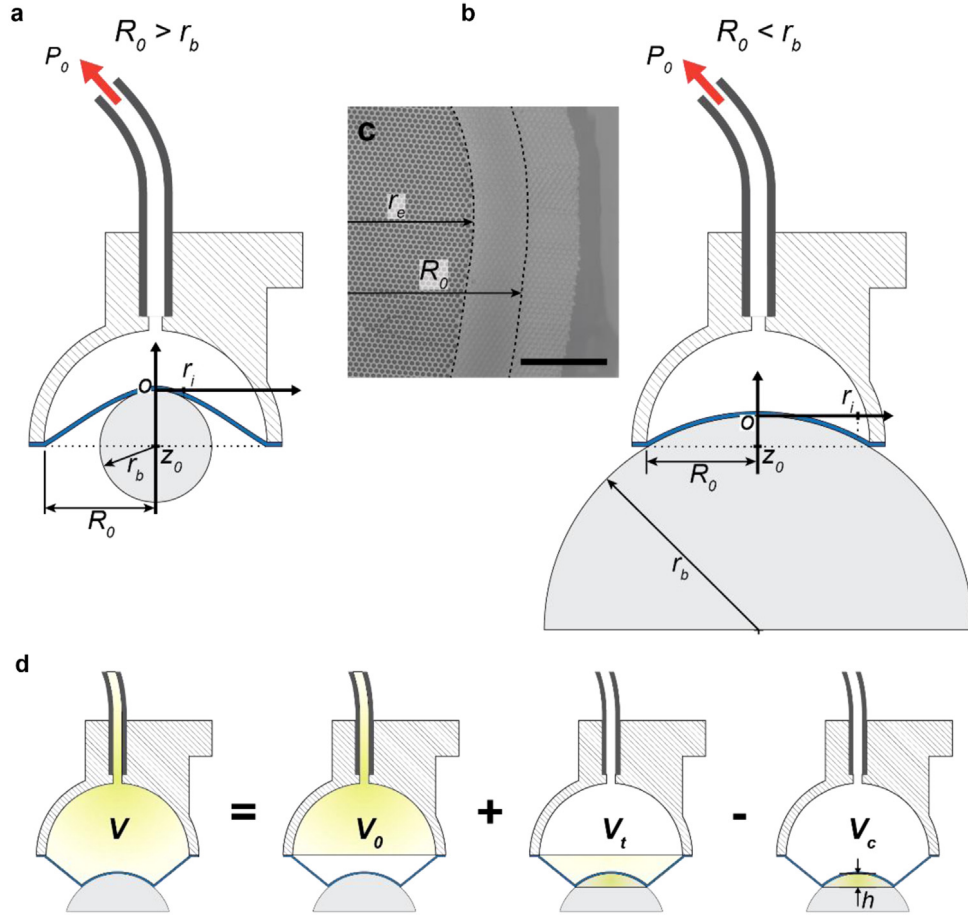
Fig. 4. Schematics for an approximate analytical model for the following cases: (**a**) the gripper is larger than a sphere ($R_0 \geq r_b$), and (**b**) vice versa ($R_0 < r_b$). (**c**) An inverted optical microscope image of the FAM at edge of the gripper in contact with a flat glass. Dots in dark gray represent microfibers in contact, while the rest of area in pale gray is not adhering to the surface. The scale bar in the image is 1 mm. (**d**) A schematic of the total volume (V) as a sum of the initial volume (V_0) added by the volume in the truncated-cone shaped deformation of the FAM (V_t), followed by a subtraction with the volume of spherical cap covered by the membrane in contact (V_c). h is the height of the spherical cap.

basic assumptions are made to further simplify the analysis as follows: (1) Fibrillar structures are ignored and the FAM will be considered as a flat membrane; (2) The FAM is incompressible; (3) The FAM is geometrically uniform over the entire area without manufacturing imperfections. Governing equations and boundary conditions are given below.

Fig. 4 shows schematics of analytical set-up for different boundary conditions depending on the size of the spherical substrates. The total potential energy of the FAM $\Pi(r^*, z^*)$ is a sum of elastic energy in the membrane, adhesion energy on the surface in contact, and work done by pressure U_p, such that

$$\Pi\left(r^*, z^*\right) = \pi \left(R_0^2 - r^{*2}\right) h_0 W_1\left(r^*, z^*\right) + \pi r^{*2} h_0 W_2\left(r^*\right) - \pi r^{*2} \omega_a + U_p\left(r^*, z^*\right). \quad (1)$$

Here, r^* is radius of the FAM in contact and z^* is corresponding position of the bottom edge of the gripper body. Also, R_0 and h_0 are radius and thickness of the FAM in the reference configuration respectively, and ω_a is the effective work of adhesion of the FAM which is approximately 4 J/m^2 on glass when measured with procedures based on the JKR model reported in [35]. $W_1(r^*, z^*)$ is the strain energy density function for which Neo-Hookean solid is assumed on the detached membrane ($r^* \leq r < R_0$), while $W_2(r^*)$ is for the part of the membrane in contact ($r < r^*$). The strain energy density function for the Neo-Hookean solid can be described as:

$$W_i\left(r^*, z^*\right) = \frac{E_m}{6}\left(\lambda_{i,\rho}^2 + \lambda_{i,\varphi}^2 + \lambda_{i,t}^2 - 3\right), \quad (i = 1, 2) \quad (2)$$

Where E_m is Young's modulus of the FAM given to be approximately 2 MPa for PDMS. Here, $\lambda_{i,\rho}$, $\lambda_{i,\varphi}$, and $\lambda_{i,t}$ are principal stretches in circumferential, meridional, and thickness for the detached ($i = 1$) and contacting ($i = 2$) portion of the FAM, respectively. Considering the truncated cone shaped deformation of the detached FAM, the principal stretches $\lambda_{1,\rho}$, $\lambda_{1,\varphi}$, and $\lambda_{1,t}$ are given as:

$$\lambda_{1,\rho} = \sqrt{\left(z^* + r_b - \sqrt{r_b^2 - r^{*2}}\right)^2 + (R_0 - r^*)^2}/(R_0 - r^*), \quad (3)$$

$\lambda_{1,\varphi} = 1$, and $\lambda_{1,t} = 1/\lambda_{1,\rho} \cdot \lambda_{1,\varphi}$.

Eq. (3) can also easily be converted for flat surface as:

$$\lambda_{1,\rho} = \sqrt{z^{*2} + (R_0 - r^*)^2}/(R_0 - r^*), \quad (4)$$

$\lambda_{1,\varphi} = 1$, and $\lambda_{1,t} = 1/\lambda_{1,\rho} \cdot \lambda_{1,\varphi}$.

Principal stretches $\lambda_{2,\rho}$, $\lambda_{2,\varphi}$, and $\lambda_{2,t}$ for spheres are given as:

$$\lambda_{2,\rho} = \frac{r_b}{r^*} \sin^{-1}\left(\frac{r^*}{r_b}\right), \lambda_{2,\varphi} = 1 \text{ and } \lambda_{2,t} = 1/\lambda_{2,\rho} \cdot \lambda_{2,\varphi}. \quad (5)$$

The principal stretches $\lambda_{2,\rho}$, $\lambda_{2,\varphi}$, and $\lambda_{2,t}$ for a flat surface will be zero, as the reference configuration in contact area remains flat. The work done by pressure U_p in Eq. (1) is given as:

$$U_p\left(r^*, z^*\right) = P_{atm}\left(V\left(r^*, z^*\right) - V_0\right) - \left(P_{atm} + P_0\right) V_0 \ln\left(V\left(r^*, z^*\right)/V_0\right), \quad (6)$$
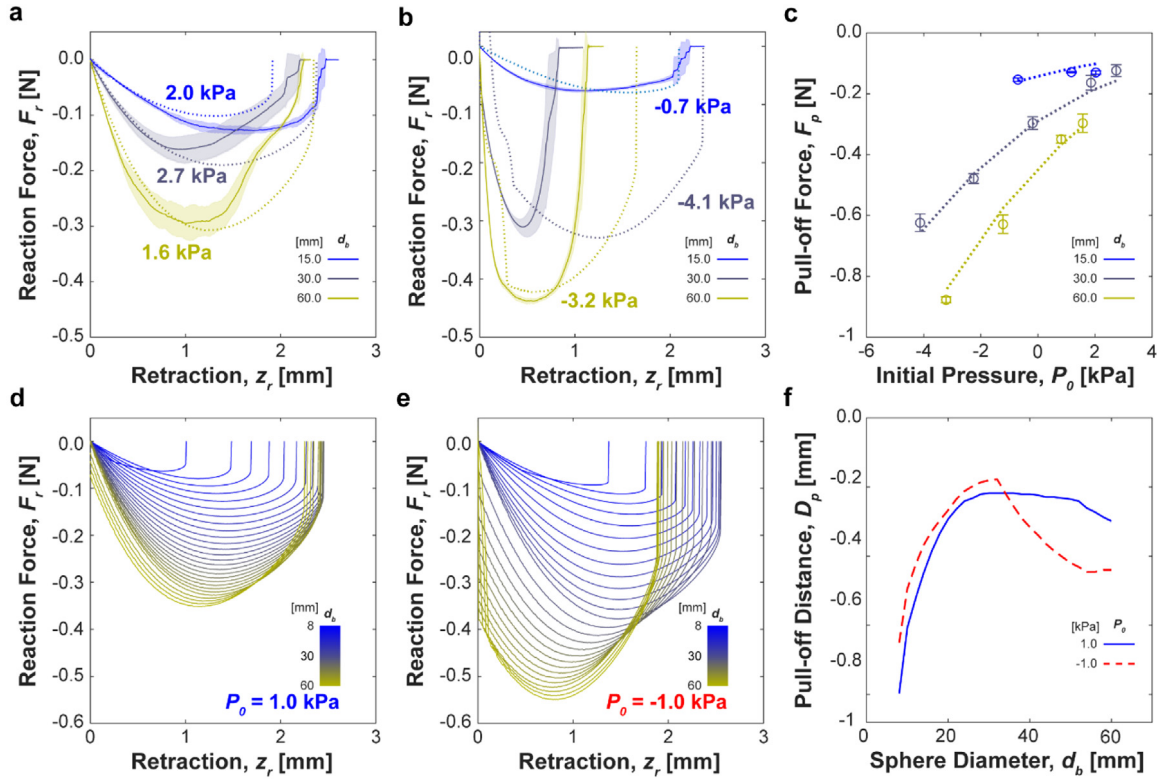
Fig. 5. Experimental and theoretical reaction force profiles (F_r) of the PDMS-based FAM with respect to retraction (z_r) depending on size of spherical substrates under similar pressure conditions: (**a**) in case of positive initial pressure (P_0) and (**b**) negative initial pressure (P_0) at the maximum magnitude of pull-off force (F_p). Solid lines represent experimental results, while dashed lines show estimations by the theoretical model. Pressure values in the figures indicate the corresponding initial pressures and shaded areas represent standard deviations of 3–5 measurements. (**c**) Pull-off forces (F_p) of experimental results (solid circles) and theoretical predictions (dashed lines) with respect to the initial pressure (P_0). Error bars indicate standard deviations of 3–5 measurements. (**d**) Estimation of reaction force profiles (F_r) with respect to sphere diameter (d_b) ranging from 8 mm to 60 mm for initial pressure $P_0 = 1.0$ kPa and (**e**) $P_0 = -1.0$ kPa. (**f**) Estimated pull-off distance (D_p) as a function of sphere diameter (d_b) for $P_0 = 1.0$ kPa and -1.0 kPa.

where $P_{atm} = 101.3$ kPa is the atmospheric pressure, $V(r, z)$ is the air volume inside the gripper at given r and z, and V_0 is the volume when the FAM is at free-standing, which is measured to be 7.2 mL including constant volume inside the syringe and tubing. The air volume in the gripper $V(r, z)$ can be calculated by adding the volume of the truncated cone $V_t(r, z)$ to the free-standing volume V_0, followed by subtraction of the volume of the spherical cap $V_c(r)$ encapsulated by the FAM in contact (Fig. 4d):

$$V(r^*, z^*) = V_0 + V_t(r^*, z^*) - V_c(r^*). \tag{7}$$

The volume of the spherical cap $V_c(r)$ and truncated cone $V_t(r, z)$ are given as:

$$V_c(r^*) = \frac{\pi h}{6}\left(3r^{*2} + h^2\right) \text{ and}$$
$$V_t(r^*, z^*) = \frac{\pi}{3}(z^* + h)\left(R_0^2 + r^{*2} + R_0 r^*\right). \tag{8}$$

The length h is the vertical distance between the FAM and the top of sphere as shown in Fig. 4d and given as:

$$h = r_b - \sqrt{r_b^2 - r^{*2}}. \tag{9}$$

In the case of a flat surface, $V_c(r)$ becomes zero, as there is no h. At a given position of the FAM in z axis $z = z^*$, the maximum contact radius r_c satisfies the following condition that the first derivative of the total potential energy $\Pi(r, z^*)$ in Eq. (1) must be zero such that

$$\left[\frac{\partial \Pi(r, z)}{\partial r}\right]_{z=z^*} = 0. \tag{10}$$

Once the contact radius r_c at the gripper height z^* is known, the reaction force (F_r) can be calculated by evaluating the first derivative of the total potential energy at (r_c, z^*):

$$F_r(z^*) = \frac{\partial \Pi(r_c, z^*)}{\partial z}. \tag{11}$$

Unlike flat surfaces, spherical substrates require an additional boundary condition related to the initial gripper position (z_0) in order to calculate the reaction force (F_r) from Eq. (11). As already discussed in Fig. 2a, the initial gripper position in the experiments is determined based on the compressive preload acting on the FAM during indentation. For calculation of the reaction force, however, it is not possible to determine the initial gripper position (z_0) based on the preload. Therefore, to simplify the contact problem during pre-loading, we assume the initial position of the gripper based on geometrical relationships between the gripper and the spherical substrates. As shown in Fig. 4a, the bottom plane of the gripper body approaches to the center of the sphere for cases in which the gripper is larger than the sphere ($R_0 \geq r_b$). For cases when the sphere is larger than the gripper, as seen in Fig. 4b ($R_0 < r_b$), the gripper is assumed to be brought down to the sphere until its rim touches the substrate. Based on the above assumption and using geometrical relationships between the gripper and the spheres, the initial gripper position z_0 as well as initial contact radius r_i can be described as

$$z_0 = -r_b \text{ and } r_i = \frac{r_b^2}{R_0} \ (R_0 \geq r_b); \tag{12}$$

$$z_0 = -r_b + \sqrt{r_b^2 - R_0^2} \text{ and } r_i = r_e \ (R_0 < r_b). \tag{13}$$
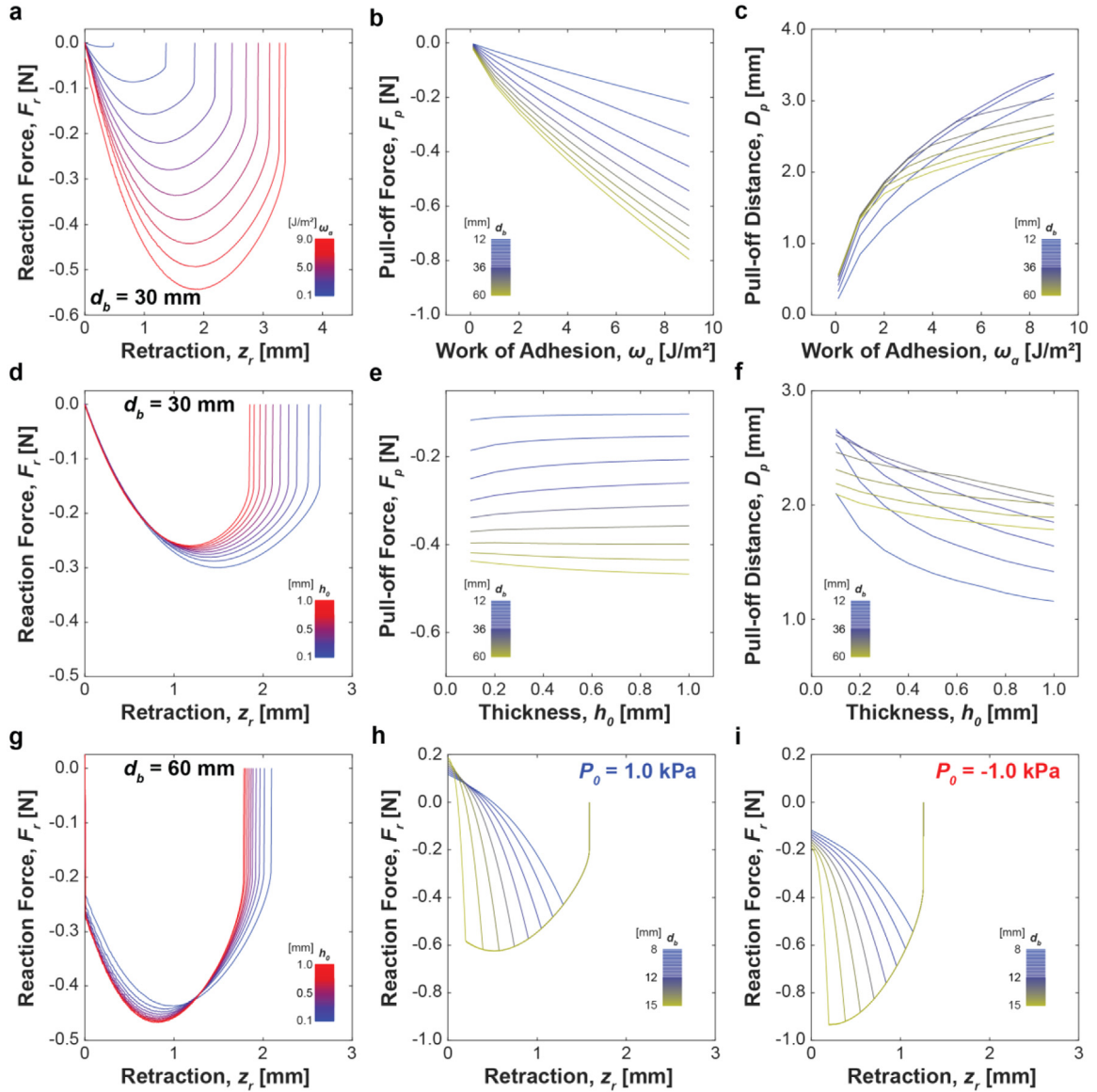
Fig. 6. Model predictions of the effect of various design parameters on reaction force profiles (F_r) of the FAM: estimation of the effect of work of adhesion (ω_a) on (**a**) reaction force profiles (F_r), (**b**) pull-off force (F_p), and pull-off distance (D_p) (**c**) at sphere diameter (d_b) ranging from $d_b = 12$ mm to $d_b = 60$ mm. The work of adhesion (ω_a) varies in range from 0.1 J/m² to 9.0 J/m², and the sphere diameter $d_b = 30$ mm in (a). Estimation of the effect of membrane thickness (h_0) on (**d, g**) reaction force profiles (F_r), (**e**) pull-off force (F_p), and (**f**) pull-off distance (D_p) at sphere diameter (d_b) ranging from $d_b = 12$ mm to $d_b = 60$ mm. The membrane thickness (h_0) varies in range from 0.1 mm to 1.0 mm, and the sphere diameter $d_b = 30$ mm in (d) and $d_b = 60$ mm in (g). Reaction force profiles (F_r) depending on the size of flat glass disks (d_b) ranging from $d_b = 8$ mm to $d_b = 15$ mm (full contact) predicted at (**h**) $P_0 = 1.0$ kPa, and (**i**) $P_0 = -1.0$ kPa.

Note that the FAM cannot achieve the initial contact radius (r_i) up to the size of gripper radius (R_0) due to manufacturing imperfection. The effective radius at full contact (r_e) is determined experimentally based on microscopic observation as shown in Fig. 4c. Therefore, we also assume the following boundary condition:

$$z_0 = -r_b \text{ and } r_i = r_e \ (r_b < R_0 \leq \frac{r_b^2}{r_e}). \tag{14}$$

When retracting the FAM from the initial indentation point (z_0), the calculated reaction force (F_r) with respect to the gripper height (z) begins at a high positive reaction force (compression). By replotting the reaction force (F_r) with respect to retraction (z_r) accounting for negative reaction force (adhesion), the calculated profiles can be compared to the experimental results. As seen in Fig. 5a, estimation of F_r using the proposed model matches reasonably with the experimental results when the FAM undergoes positive initial pressure (P_0). An average deviation of

the model in predicting pull-off distance (D_p) was 9% from our experimental results in the sphere diameter 15, 30, and 60 mm. However, as shown for the case of $d_b = 30$ mm and 60 mm (Fig. 5b), the deviation increases when the membrane is exposed to a high negative pressure differential. The model predicts D_p in average approximately 1.7 times longer than the experimental results, and 2.8 times at maximum in case of $d_b = 30$ mm. This comparison indicates that the proposed model based on the assumption of a truncated cone shaped deformation could be more accurate in estimating the force profiles when the FAM is not exposed to a high negative pressure differential. For cases when the FAM is exposed to a high negative initial pressure, the truncated cone is no longer a valid assumption for the shape of the membrane, since the detached portion of the membrane deforms towards the inside of the gripper in a shape similar to a toroid. The toroidal shape deformation causes greater stretch in the membrane than that of the truncated cone shape, resulting

in a higher line tension. This causes the FAM to detach from the substrate faster than the current model predictions. Although the predicted shape of reaction force deviates from experimental results under the high negative initial pressure, the estimated pull-off forces are reasonably accurate for a wide range of positive and negative initial pressure with an average deviation of 9% as shown in Fig. 5c. Considering 12% of the average deviation in our previous model [35] for spherical substrates, the consideration of membrane deformation on the adhering membrane using the strain energy density function W_2 in Eq. (1) better describes the mechanics of membrane adhesion, improving the accuracy in pull-off force prediction.

The advance and retreat of the pull-off distance (D_p) in the reaction force profiles (F_r) of the FAM involves complex mechanics of the stress distribution on contact interface depending on the internal pressure and surface geometry. Fig. 5d and e show the estimated F_r depending on the sphere diameter (d_b) at the initial pressure $P_0 = 1.0$ kPa and $P_0 = -1.0$ kPa, respectively. As seen in both Fig. 5d and e, D_p initially advances with respect to the increased d_b due to the expansion of contact area as well as the decrease in radius of curvature. According to the model, D_p reaches the maximum at $d_b = 32$ mm, then retreats with respect to the increased d_b. A similar behavior was observed in our experimental results with the polyurethane-based FAM in **Fig. S2**. As seen in Fig. 5f, a negative P_0 amplifies the reduction in D_p by almost 26% from the maximum at $d_b = 32$ mm to $d_b = 60$ mm, while there is only 8% decrease in D_p at $d_b = 60$ mm when $P_0 = 1.0$ kPa.

The model predicts an increase in D_p under a negative $P_0 = -1.0$ kPa in Fig. 5f, comparing to $P_0 = 1.0$ kPa, when d_b is smaller than 32 mm. As seen in Fig. 3a, we also observed the advance of D_p with respect to the decreased P_0 at $d_b = 15$ mm. A negative P_0 can utilize the entire contact area by equal load sharing, increasing the effective work of adhesion. At the same time, the negative P_0 causes a high stress concentration at the contact edge. We speculate that the increase in stress concentration at the contact edge under the negative P_0 can be negligible at a small d_b, due to a short length of the circumferential edge; in this case, the effect of load sharing which increases the work of adhesion is dominant, resulting the increase in magnitude of both F_p and D_p as shown in Fig. 6a. In case of a large d_b, on the other hand, the stress concentration at a long contact edge plays a major role in the peeling of the membrane; while the negative P_0 still increases the work of adhesion over the entire contact area, the high stress concentration at the contact edge can peel off the membrane with a shorter D_p, as observed in Fig. 3b and c.

Fig. 6 shows the effect of various design parameters, such as the work of adhesion (ω_a), membrane thickness (h_0), and surface geometry on the adhesion of the FAM. As seen in Fig. 6a, both pull-off force (F_p) and pull-off distance (D_p) monotonically increase with respect to the increased ω_a; however, the effect of ω_a in improving F_p is negligible for a small sphere diameter (d_b) as shown in Fig. 6b. Also, the slope in D_p decreases with respect to the increased ω_a as shown in Fig. 6c. The reaction force profiles (F_r) in Fig. 6d and g show a competing effect between restoring force and equal load sharing with h_0 as a function of sphere diameter. On a small d_b with a large radius of curvature shown in Fig. 6d, a thicker membrane in contact has a high restoring force due to its elasticity, resulting in a decreased F_p, as discussed by Majidi and Fearing [43]. On a large d_b with a small radius of curvature shown in Fig. 6g, on the other hand, a better load sharing due to the increased effective stiffness, caused by the thicker membrane, overcomes the effect of the increased restoring force, resulting in a higher magnitude of F_p (Fig. 6e). Regardless of the size of d_b, however, D_p always decreases when h_0 increases, according to our model prediction shown in Fig. 6f.

Applying our model for flat surfaces, we calculated F_r for different sizes of flat glass disks ranging from $d_b = 8$ mm to $d_b = 15$ mm as shown in Fig. 6h and i. The model predicts the influence of initial pressure (P_0) on F_p and D_p similar to the case of spherical surfaces; a decrease in P_0 mainly causes a higher magnitude of F_p ($F_p = -0.62$ N at maximum in Fig. 6h, while $F_p = -0.94$ N at maximum in Fig. 6i.) and a shorter D_p ($D_p = 1.59$ mm in Fig. 6h, while $D_p = 1.26$ mm in Fig. 6i). On the other hand, the diameter of the flat contact area d_b attributes to the slope of F_r during retraction; a larger d_b results a stiffer decrease in F_r when the gripper is retracted, although a change in d_b does not make a difference in D_p under the same P_0.

Although predictions made by the proposed model may not quantitatively match with experiments due to some simplifying assumptions, our model can nonetheless provide interesting insights. Such insights are related to the sophisticated behavior of the adhesion mechanics of an elastic membrane when taking multiple boundary conditions into account. Therefore, the theoretical model presented in this paper can be employed for high accuracy pull-off force estimations of a membrane together with a qualitative estimation of force profiles under various boundary conditions.

5. Conclusion

In this paper, we discuss the mechanics of an adhering membrane undergoing complex boundary conditions, focusing especially on a membrane being pulled off from a non-planar spherical surface under a pressure differential. The Fiber Adhesives on a Membrane (FAM) design allows for reliable and repetitive attachment and detachment cycles, while eliminating any contribution of undesired forces (i.e., suction or capillary forces) to adhesion. Experimental results show that the negative pressure differential across the FAM increases the pull-off force by the effect of equal load sharing on substrates with a wide range of radii of curvature, as if the backing layer is stiffened. Furthermore, we find that size and curvature of surfaces affect the reaction force profiles of the membrane. A higher pull-off force is obtained at shorter retraction distances, when engaging a larger sphere with smaller radius of curvature. An approximate theoretical model based on principle of the minimum potential energy is further improved from our previous work [35], showing a higher accuracy in predicting pull-off force. We show that it can provide basic understanding of how an adhesive membrane behaves under the complex boundary changes, and predict its pull-off force with high accuracy. Although we used the FAM system as a test platform to investigate the adhesion mechanics of a membrane, the insights gained from this study can be applied to general problems in the membrane adhesion for a wide variety of scientific and engineering fields, regardless of whether the membrane is structured or not. For future work, the model accuracy under a high negative pressure differential can be improved by incorporating more accurate theoretical estimation on shape of the deformed membrane based on constitutive equations and balance laws. Moreover, these soft grippers will be used to pick-and-place a variety of curved objects for transfer printing and robotic manipulation applications as a future work.

Appendix A. Supplementary data

Supplementary material related to this article can be found online at https://doi.org/10.1016/j.eml.2019.100485.

References

[1] K. Kendall, Thin-film peeling-the elastic term, J. Phys. D 8 (1975) 1449–1452.

[2] D. Labonte, C.J. Clemente, A. Dittrich, Extreme positive allometry of animal adhesive pads and the size limits of adhesion-based climbing, Proc. Nat. Acad. Sci. 113 (2016) 1297–1302.

[3] N.S. Pesika, Y. Tian, B. Zhao, K. Rosenberg, H. Zeng, P. McGuiggan, et al., Peel-zone model of tape peeling based on the gecko adhesive system, J. Adhes. 83 (2007) 383–401.

[4] D. Labonte, W. Federle, Scaling and biomechanics of surface attachment in climbing animals, Philos. Trans. R. Soc. B 370 (2015) 20140027.

[5] Y. Tian, N. Pesika, H. Zeng, K. Rosenberg, B. Zhao, P. McGuiggan, et al., Adhesion and friction in gecko toe attachment and detachment, Proc. Nat. Acad. Sci. 103 (2006) 19320–19325.

[6] E.A. Evans, D.A. Calderwood, Forces and bond dynamics in cell adhesion, Science 316 (2007) 1148–1153.

[7] A. Sancho, I. Vandersmissen, S. Craps, A. Luttun, J. Groll, A new strategy to measure intercellular adhesion forces in mature cell–cell contacts, Sci. Rep. 7 (2017) 46152.

[8] R. Winklbauer, Cell adhesion strength from cortical tension - an integration of concepts, J. Cell Sci. 128 (2015) 3687–3693.

[9] A. Carlson, H.-J. Kim-Lee, J. Wu, P. Elvikis, H. Cheng, A. Kovalsky, et al., Shear-enhanced adhesiveless transfer printing for use in deterministic materials assembly, Appl. Phys. Lett. 98 (2011) 264104.

[10] S.Y. Yang, A. Carlson, H. Cheng, Q. Yu, N. Ahmed, J. Wu, et al., Elastomer surfaces with directionally dependent adhesion strength and their use in transfer printing with continuous roll-to-roll applications, Adv. Mater. 24 (2012) 2117–2122.

[11] Q. Xu, Y. Wan, T.S. Hu, T.X. Liu, D. Tao, P.H. Niewiarowski, et al., Robust self-cleaning and micromanipulation capabilities of gecko spatulae and their bio-mimics, Nat. Commun. 6 (2015) 8949.

[12] Y. Mengüç, S.Y. Yang, S. Kim, J.A. Rogers, M. Sitti, Gecko-inspired controllable adhesive structures applied to micromanipulation, Adv. Funct. Mater. 22 (2012) 1246–1254.

[13] H. Prahlad, R. Pelrine, S. Stanford, J. Marlow, R. Kornbluh, Electroadhesive robots—wall climbing robots enabled by a novel, robust, and electrically controllable adhesion technology, Proc. IEEE International Conference on Robotics and Automation, 2008, pp. 3028–3033.

[14] J. Shintake, S. Rosset, B. Schubert, D. Floreano, H. Shea, Versatile soft grippers with intrinsic electroadhesion based on multifunctional polymer actuators, Adv. Mater. 28 (2015) 231–238.

[15] M.P. Murphy, C. Kute, Y. Mengüç, M. Sitti, Waalbot II: Adhesion recovery and improved performance of a climbing robot using fibrillar adhesives, Int. J. Robot. Res. 30 (2011) 118–133.

[16] O. Unver, M. Sitti, Tankbot: A palm-size, tank-like climbing robot using soft elastomer adhesive treads, Int. J. Robot. Res. 29 (2010) 1761–1777.

[17] E.W. Hawkes, E.V. Eason, D.L. Christensen, M.R. Cutkosky, Human climbing with efficiently scaled gecko-inspired dry adhesives, J. R. Soc. Interface 12 (2014) 20140675.

[18] S. Kim, M. Spenko, S. Trujillo, B. Heyneman, D. Santos, M.R. Cutkosky, Smooth vertical surface climbing with directional adhesion, IEEE Trans. Robot. 24 (2008) 65–74.

[19] A.L. Flory, D.A. Brass, K.R. Shull, Deformation and adhesive contact of elastomeric membranes, J. Polym. Sci. B 45 (2007) 3361–3374.

[20] R. Long, K.R. Shull, C.-Y. Hui, Large deformation adhesive contact mechanics of circular membranes with a flat rigid substrate, J. Mech. Phys. Solids 58 (2010) 1225–1242.

[21] R. Long, C.-Y. Hui, Axisymmetric membrane in adhesive contact with rigid substrates: Analytical solutions under large deformation, Int. J. Solids Struct. 49 (2012) 672–683.

[22] D. Xu, K.M. Liechti, Analytical and experimental study of a circular membrane in adhesive contact with a rigid substrate, Int. J. Solids Struct. 48 (2011) 2965–2976.

[23] E.J. Laprade, R. Long, J.T. Pham, J. Lawrence, T. Emrick, A.J. Crosby, et al., Large deformation and adhesive contact studies of axisymmetric membranes, Langmuir 29 (2013) 1407–1419.

[24] A. Srivastava, C.Y. Hui, Large deformation contact mechanics of a pressurized long rectangular membrane. II. Adhesive contact, Proc. R. Soc. A 469 (2013) 20130425.

[25] M. Shanahan, Adhesion of a punch to a thin membrane, C. R. Acad. Sci. Ser. IV 1 (2000) 517–522.

[26] K.T. Wan, Adherence of an axisymmetric flat punch onto a clamped circular plate: Transition from a rigid plate to a flexible membrane, J. Appl. Mech. 69 (2001) 110–116.

[27] C. Majidi, R.E. Groff, R.S. Fearing, Analysis of shaft-loaded membrane delamination using stationary principles, Math. Mech. Solids 13 (2007) 3–22.

[28] J. Shi, S. Müftü, K.-T. Wan, Adhesion of an elastic convex shell onto a rigid plate, J. Adhes. 87 (2011) 579–594.

[29] B.-F. Ju, Y. Ju, M. Saka, K.-K. Liu, K.-T. Wan, A systematic method for characterizing the elastic properties and adhesion of a thin polymer membrane, Int. J. Mech. Sci. 47 (2005) 319–332.

[30] A. Patil, A. DasGupta, A. Eriksson, Contact mechanics of a circular membrane inflated against a deformable substrate, Int. J. Solids Struct. 67–68 (2015) 250–262.

[31] A. Patil, A. Nordmark, A. Eriksson, Free and constrained inflation of a pre-stretched cylindrical membrane, Proc. R. Soc. A 470 (2014) 20140282.

[32] R.M. Springman, J.L. Bassani, Mechano-chemical coupling in the adhesion of thin-shell structures, J. Mech. Phys. Solids 57 (2009) 909–931.

[33] S. Song, M. Sitti, Soft grippers using micro-fibrillar adhesives for transfer printing, Adv. Mater. 26 (2014) 4901–4906.

[34] S. Song, C. Majidi, M. Sitti, GeckoGripper: A soft, inflatable robotic gripper using gecko-inspired elastomer micro-fiber adhesives, Proc. IEEE/RSJ International Conference on Intelligent Robots and Systems, 2014, pp. 4624–4629.

[35] S. Song, D.-M. Drotlef, C. Majidi, M. Sitti, Controllable load sharing for soft adhesive interfaces on three-dimensional surfaces, Proc. Natl. Acad. Sci. 114 (2017) E4344–E4353.

[36] M.P. Murphy, B. Aksak, M. Sitti, Adhesion and anisotropic friction enhancements of angled heterogeneous micro-fiber arrays with spherical and spatula tips, J. Adhes. Sci. Technol. 21 (2007) 1281–1296.

[37] M.P. Murphy, B. Aksak, M. Sitti, Gecko-inspired directional and controllable adhesion, Small 5 (2008) 170–175.

[38] M.P. Murphy, S. Kim, M. Sitti, Enhanced adhesion by gecko-inspired hierarchical fibrillar adhesives, ACS Appl. Mater. Interfaces 1 (2009) 849–855.

[39] A.G. Gillies, J. Puthoff, M.J. Cohen, K. Autumn, R.S. Fearing, Dry self-cleaning properties of hard and soft fibrillar structures, ACS Appl. Mater. Interfaces 5 (2013) 6081–6088.

[40] Y. Mengüç, M. Röhrig, U. Abusomwan, H. Hölscher, M. Sitti, Staying sticky: contact self-cleaning of gecko-inspired adhesives, J. R. Soc. Interface 11 (2014) 20131205.

[41] S. Kim, E. Cheung, M. Sitti, Wet self-cleaning of biologically inspired elastomer mushroom shaped microfibrillar adhesives, Langmuir 25 (2009) 7196–7199.

[42] N.C. Goulbourne, E.M. Mockensturm, M.I. Frecker, Electro-elastomers: Large deformation analysis of silicone membranes, Int. J. Solids Struct. 44 (2007) 2609–2626.

[43] C. Majidi, R.S. Fearing, Adhesion of an elastic plate to a sphere, Proc. R. Soc. A 464 (2008) 1309–1317.